J Mol Model (2011) 17:1075–1080
DOI 10.1007/s00894-010-0814-5

ORIGINAL PAPER

Theoretical investigation of ZnO and its doping clusters

Chunlei Wang · Shuhong Xu · Lihua Ye · Wei Lei · Yiping Cui

Received: 27 June 2010 / Accepted: 15 July 2010 / Published online: 28 July 2010

Abstract Four clusters of ZnO, O–Zn–SR (–SR = ligand) and doping ZnO structures (with Cr, Cu, Al atoms) were investigated using density functional theory at theB3LYP/Lanl2dz level. The characteristics of Zn_3O_3 and Zn_4O_4 structures, which are the units of experimental wurtzite and zinc blende structures, were found to be similar to those of experimental ZnO nanocrystals. Moreover, the calculated Raman and IR spectra of ZnO clusters were almost consistent with experimental results. Raman spectra were observed to shift to higher frequencies with decreasing numbers of atoms. Both ligands and solvent make the wavelength of absorption peaks shift to blue. All transitions of absorption peaks for these pure clusters were from d to p orbitals. Finally, doping clusters and experimental doping nanocrystals were similar in character. The doping of metal changed the orbital of ZnO nanocrystals. The transitions in doping clusters (Cr–ZnO, Cu–ZnO) are from d to d orbitals, while Al–ZnO clusters have s–p transitions.

Keywords Raman spectra · IR spectra · Doping cluster · Absorption spectra

Introduction

Zinc oxide is a semiconductor material well-known for its wide band gap and high exciton binding energy at room temperature. Recently, ZnO nanostructures have attracted increasing attention due to their potential application in laser diodes, blue lasing media and other optoelectronic devices. Experimentally, ZnO has been synthesized using physical and chemical methods [1–4]. Simultaneously, the UV spectra, Raman spectra, IR spectra and photoluminescence of these compounds have been investigated. The group of P.G. Yin studied photoluminescence spectra, non-resonant and resonant Raman scattering spectra, and IR spectra with ZnO nanorods synthesized by a simple method [5], and proved that normal Raman spectra, at both low and high frequency vibrations, supported the perfect wurtzite structure of ZnO nanorods. Additionally, they confirmed that the red shift and broadening of vibrational modes were due mainly to the laser irradiation effect. The electronic properties of undoped bulk ZnO and well aligned ZnO nanorods have been investigated using micro Raman spectroscopy [6]. Xue [7] reported the room temperature ferromagnetism of pure ZnO nanoparticles prepared using a coprecipitation method. The optical anisotropy of below- and above-band-edge transitions in three samples of well-aligned and titled ZnO nanorods has been characterized using thermoreflectance and photoluminescence measurements in the temperature range between 30 and 300 K [8]. Raman and emission properties under different excitation wavelengths have been studied at the nanoscale [9]. Low-frequency Raman spectrometry revealed acoustic phonons in wurtzite prismatic zinc oxide nanoparticles of sizes varying from 2.3 to 6.6 nm, together with a Raman spectra shift toward higher frequencies with a decrease in nanoparticle size [10].

Doped ZnO clusters, such as Zn(Mn)O [11–13], Zn(Co)O [14–17], Zn(Cu)O [18], Zn(Al)O [19, 20], are currently a hotspot of research. The wavelengths of luminescence, magnetism and orbitals of these types of doping nanocrystals differ from those of pure ZnO nanocrystals, which widens the potential for their application. UV and Raman

C. Wang · S. Xu · L. Ye · W. Lei · Y. Cui (✉)
Advanced Photonics Center, School of Electronic Science and Engineering, Southeast University,
Nanjing 210096, China
e-mail: cyp@seu.edu.cn

spectra characteristics of these doped structures have also been studied. In a theoretical study in 2006, the magnetic properties of transition metal (Mn, Co and Ni) doped ZnO were determined by an embedded cluster approach using ab initio methods [21, 22]. The energies, stable configurations and electronic structures of $(ZnO)_n$ clusters for n ranging from 9 to 64 have been studied by first-principles calculations [23].

More recently, density functional theory (DFT) has been used to study small ZnO clusters [24]. This method was used to investigate the energies and configurations of stoichiometric $(ZnO)_n$ clusters on a graphite surface [25]. The structural and electronic characterization of n-doped (Al and In) ZnO and the effect of the doping on the calculated photoelectron spectroscopy spectra have been presented ab-initio [26].

Thus, although the geometric parameters of ZnO clusters have been calculated before, the influence of solvent and ligand has always been ignored, thus the calculated characters (Raman spectra, absorption spectra, molecular orbital) of these clusters differ from experimental results. In other words, comparison of experiment and theory has not yet been established. In the current work, by considering the integration effect of solvent and ligand, the absorption spectra of ZnO clusters were rationalized and compared with experimental results taking into account quantum size effects. Moreover, using our chosen method (DFTBLYP/Lanl2dz) and modeling examples (four clusters), Raman and IR peaks were practically identical with reported experimental data. The absorption and IR spectra characteristics investigated in this paper have important practical implications. Therefore, the aim of the present study was to investigate the experimental characters in theory to provide guidance for further experiments.

Calculation methods

The conformations and characteristics of Zn_3O_3, $(Zn_3O_3)_2$, $(Zn_3O_3)_3$ and Zn_4O_4 along with O–Zn–SR structures were studied at DFT B3LYP/Lanl2dz level with the Gaussian03 package [27]. The electrons $1s^2 2s^2 2p^4$ for O, $3d^{10} 4s^2$ for Zn were described using the Lanl2dz basis set. With this basis set, the core electrons of Zn atoms are not taken into account. This theoretical method was designed to calculate the characteristics of Zn [28–30]. The original structures were based on the experimental zinc blende and wurtzite structures of ZnO nanocrystals. We chose seven ligands prevalent in aqueous synthesis. Molecular orbital (MO) figures were generated using the program GaussView. Because the DFT method cannot give Raman spectra, Raman spectra were calculated with keywords in this paper. The absorption spectra of the clusters were obtained using time-dependent DFT (TDDFT). In addition, solvent models were applied to obtain the properties in solvent. Ten electrostates were chosen for TDDFT calculation. The dielectric constant of water (ε) used here is 78.39. Wiberg Bond Index (WBI) values, which are used to estimate the bonding between two atoms, were calculated in natural bond orbital (NBO) with NBO keywords.

Results and discussion

Structural modeling and optimized characters

Four clusters Zn_3O_3, $(Zn_3O_3)_2$, $(Zn_3O_3)_3$ and Zn_4O_4 were optimized at B3LYP/Lanl2dz. Optimized parameters and the corresponding calculated characteristics are depicted in Fig. 1 and Table 1. Zinc blende and wurtzite structures are two common structures of ZnO nanocrystals. The main forms found in zinc blende and wurtzite are tetrahedrons and hexagons, respectively. Thus, we choose tetrahedron and hexagon as original structures. These two conformations should be similar in character to experimental ZnO nanocrystals. The Zn_3O_3 molecule is a ring with average bond lengths of 1.868 Å. However, the distance between two Zn atoms (2.916 Å) is different from that between O and O atoms (3.479 Å), making the structure of Zn_3O_3 resemble a zigzag ring. The $(Zn_3O_3)_2$ structure has two hexagons with bond lengths of 1.950 Å among the ring, and 2.080 Å between the two layers. This structure is the simplest cluster made of hexagons. $(Zn_3O_3)_3$ has three layers composed of three different hexagons. $(Zn_3O_3)_3$ resembles a tube whose wall is formed with non-planar quadrangles. The ring in the middle layer of $(Zn_3O_3)_3$ has much longer bond lengths than those in the first and second rings. Bond lengths between the two layers are longer than those among rings, namely, the distances between the two

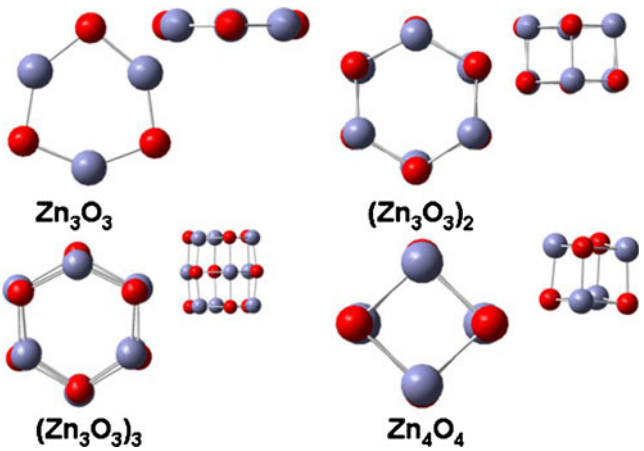

Fig. 1 Conformations of Zn_3O_3, $(Zn_3O_3)_2$, $(Zn_3O_3)_3$, Zn_4O_4 molecules

Table 1 The lowest vibrational frequencies (*Freq*), the HOMO–LUMO (*H–L*) gaps, symmetries (*Symm*), excited states (*States*), compositions of excited states (*Compos*), excited energies of singlets (ΔE) in solvent, and absorbed wavelength in water (λ), and experimental absorbed wavelength (*Exp*) for Zn_3O_3, $(Zn_3O_3)_2$, $(Zn_3O_3)_3$ and Zn_4O_4 molecules

Structure	Freq (cm^{-1})	H-L (eV)	Symm	States	Compos	ΔE (eV)	λ(W) (nm)	Exp (nm) [a]
Zn_3O_3	121	3.76	C_1	1	30 ->31	3.804	326	315
$(Zn_3O_3)_2$	93	3.46	S_6	1	60 ->61	3.438	361	
$(Zn_3O_3)_3$	84	3.59	C_1	1	90 ->91	3.418	363	
Zn_4O_4	181	2.91	C_{2V}	1	40 ->41	3.433	361	

[a] [31]

layers are longer than the bond lengths within the rings. Much longer bond lengths between the two layers in $(Zn_3O_3)_2$ and $(Zn_3O_3)_3$ clusters indicate that it is difficult for ZnO nanocrystals to form stable nanotubes. Overall, Zn and O atoms alternate in Zn_3O_3, $(Zn_3O_3)_2$ and $(Zn_3O_3)_3$ structures. Three structures have rings with six atoms. For each Zn atom, the closest neighboring atom is an O atom, and vice versa. Interestingly, Zn_4O_4—a molecule with C_{2V} symmetry—has a different conformation. The Zn atom forms a tetrahedron with O atoms, which also form a tetrahedron with Zn atoms. Bond lengths between the two quadrangles are 2.025 Å, and those within the quadrangles are 2.022 Å. The Zn_4O_4 structure resembles that of zinc blende, which is another main constitution of ZnO nanocrystals.

Raman spectra of Zn_3O_3, $(Zn_3O_3)_2$ and $(Zn_3O_3)_3$ (Fig. 2), and IR and Raman spectra of Zn_4O_4 (Fig. 3) were calculated at B3LYP/Lanl2dz level. As can be seen from Fig. 2, the most intensive Raman peaks of Zn_3O_3, $(Zn_3O_3)_2$ and $(Zn_3O_3)_3$ are at 502, 252 and 245 cm^{-1}, respectively. Clearly, there is a shift toward higher frequencies with a decrease in the size of clusters, which is exactly what is observed experimentally [26]. The most intensive Raman peak of Zn_4O_4 appears at 286 cm^{-1}, and its IR peak is at 445 cm^{-1}, which is almost identical with the experimental result (439 cm^{-1}) reported by Yin's group [5]. Moreover, the shift to higher frequencies seen with the calculated data can be deduced from the above rule as the sizes of our clusters are smaller than those of experimental nanocrystals. The frequencies of the highest Raman peak for the four clusters also shift to low frequencies with the increase in the number of atoms.

We next calculated absorption spectra at B3LYP/Lanl2dz level by the TDDFT method. The wavelengths of absorption peaks shift towards red in the order Zn_3O_3, $(Zn_3O_3)_2$ and $(Zn_3O_3)_3$, which is induced by a quantum size effect. Moreover, the wavelengths of the absorption peaks of our clusters are shorter than those of bulk ZnO (band gap energy of 3.20 eV) because our clusters are smaller in size than bulk ZnO materials, which is also consistent with a quantum size effect. However, compared with those of experimental ZnO nanocrystals, our calculated wavelengths of the absorption spectra of clusters are shifted towards the red end of the spectrum. This is because our calculations do not consider the influence of the ligand. Highest occupied molecular orbital (HOMO) and lowest unoccupied molecular orbital (LUMO) are depicted in Fig. 4. HOMO–LUMO gap data shows that all these clusters are semiconductors. The illustrations of the four clusters shows that the d orbital makes a significant contribution to HOMO; conversely, there is no d orbital in the LUMO, which is instead composed of p orbital. Thus, the transitions in ZnO nanocrystals are from d to p orbitals.

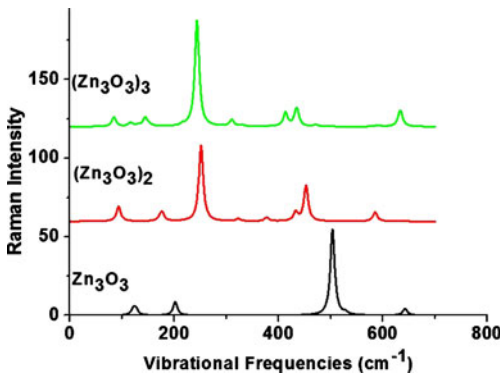

Fig. 2 Raman spectra of Zn_3O_3, $(Zn_3O_3)_2$ and $(Zn_3O_3)_3$ molecules

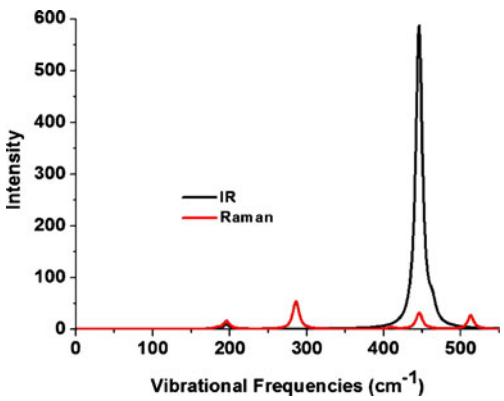

Fig. 3 IR spectra and Raman spectra of Zn_4O_4 molecule

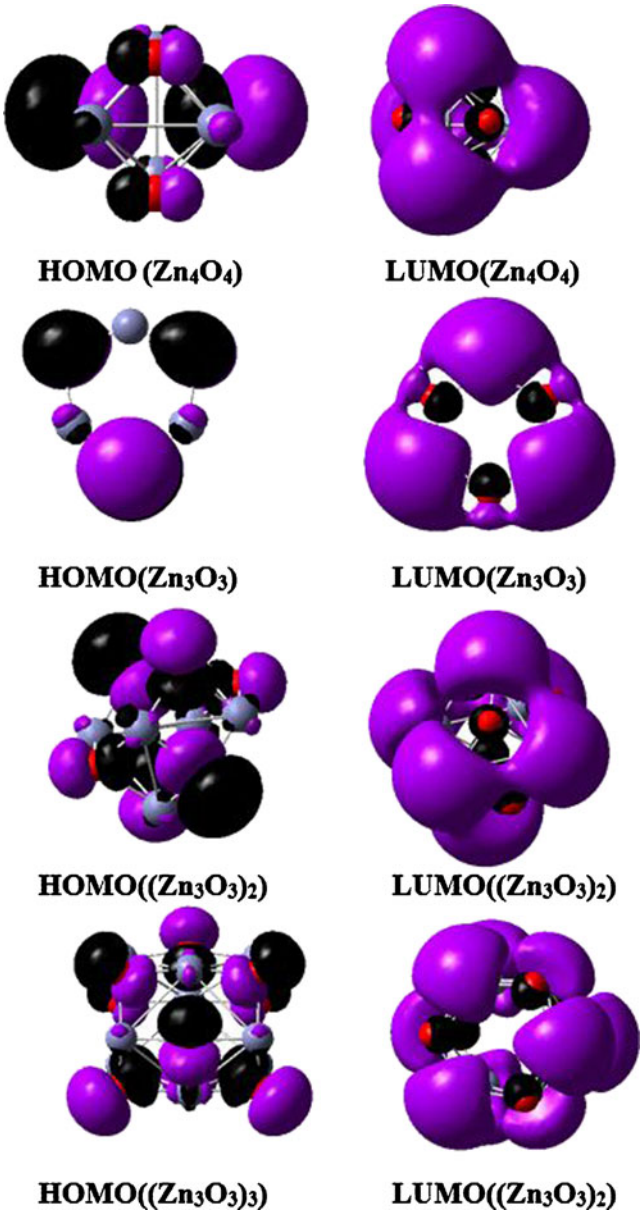

Fig. 4 Highest occupied molecular orbital (HOMO) and lowest unoccupied molecular orbital (LUMO) figures of Zn_4O_4, Zn_3O_3, $(Zn_3O_3)_2$ and $(Zn_3O_3)_3$ molecules

The influence of ligand and their bonds in ZnO clusters

All the following ligands are familiar in aqueous synthesis: $-CH_2-CH_2-COOH$, $-CH_2-CH_2-N(CH_3)_2$, $-CH_2-CH_2-NH_2$, $-CH_2-CH_2(OH)$, $-CH_2-CH(NH_2)-COOH$, $-CH_2-CH(OH)-CH_2(OH)$ and $-CH_2-COOH$ (Table 2). Additionally, many ligands in aqueous synthesis contain thiol. In this study, we chose these types of ligands to investigate the effect of ligands under aqueous conditions. First, we found that bond lengths of O–Zn in O–Zn–SR structures are longer than the bond length of the ZnO unit, viz. the ligands weaken the bond between O and Zn. We can also say that bonds in ZnO nanocrystals differ from those in ZnO bulk materials; ZnO nanocrystals have weaker bonds than ZnO bulk material. Second, bonding, absorption spectra and the lowest frequencies of seven O–Zn–SR structures exhibited no obvious difference. Moreover, O–Zn–SR with $–S–CH_2–CH_2–NH_2$ and $–S–CH_2–CH_2$ (OH) ligands have almost the same bond lengths and absorption wavelengths. Therefore, we assume that, in practical experiments, all ligands have a similar influence on ZnO nanocrystals. $–S–CH_2–CH_2–NH_2$ and $–S–CH_2–CH_2$ (OH) ligands should have the same influence on ZnO nanocrystals. All these ligands are used in aqueous synthesis experimentally, and ZnO nanocrystals with SR have similar characteristics as they all contain thiols. Certainly, the composition and electronic character of R have some influence on ZnO nanocrystals. Clearly, in theoretical calculations, ZnO nanocrystals with seven ligands essentially do not differ, which is identical with experimental results. Third, comparing absorption wavelengths of O–Zn–SR clusters in solvent and gas phase, we found that the presence of solvent causes a shift in the absorption wavelengths towards blue. We found that ligands also confer a blue shift on absorption wavelengths. In this way, the wavelengths of absorption peaks of the above four clusters will shift to blue upon addition of ligands. In other words, under these conditions (with solvent and ligands), the calculated absorption wavelengths are close to

Table 2 The lowest vibrational frequencies (cm^{-1}), absorption spectra in solvent (nm), bond lengths (B-L) (Å) and Wiberg Bond Index (WBI) values for O–Zn–ligand molecules

O-Zn-SR	Freq (cm^{-1})	λ(W) (nm)	B-L(Å) O-Zn	B-L(Å) Zn-S	WBI O-Zn	WBI Zn-S
O-Zn	698	449	1.764	——	1.21	——
O-Zn-S-CH_2-CH_2-COOH	16	277	1.881	2.281	0.41	0.56
O-Zn-S-CH_2-CH_2-$N(CH_3)_2$	23	278	1.882	2.274	0.41	0.56
O-Zn-S-CH_2-CH_2-NH_2	59	255	1.904	2.333	0.36	0.42
O-Zn-S-CH_2-CH_2(OH)	73	261	1.899	2.329	0.37	0.43
O-Zn-S-CH_2-CH(NH2)-COOH	17	322	1.882	2.281	0.41	0.56
O-Zn-S-CH_2-CH(OH)-CH_2(OH)	20	275	1.880	2.276	0.41	0.53
O-Zn-S-CH_2-COOH	28	271	1.879	2.289	0.41	0.56

experimental results, according to quantum size effect. Through analysis of Raman spectra of O–Zn–SR, we detect that the whole O–Zn–S does not vibrate except for O–Zn–S–CH_2–CH_2–NH_2 and O–Zn–S–CH_2–CH_2–OH structures, i.e., the ligand makes the ZnO nanocrystals stable (also a function of ligand s known from experimental data). Finally, the WBI value of NBO shows that Zn has a stronger bond with the ligand than between Zn and O. Thus, it is difficult to synthesize ZnO nanocrystals in aqueous phase.

Characteristics of doped ZnO clusters

Characteristics of Cr-, Cu- and Al-doped ZnO clusters were investigated at the B3LYP/Lanl2dz level. The WBI value of NBO is a useful method to study the bonds among atoms. In this paper, we use WBI values to judge the bonds in these doped clusters. As with Cr–ZnO clusters, the bond between Cr and O atoms is stronger than that between Zn and O atoms. Moreover, only a very weak bond exists between Zn and Cr atoms in some structures. In Zn_2–Cr_2–O_4, two Cr atoms have a strong bond, with WBI value 1.3. From this information, we estimate that there is metal–metal bond in some ZnO nanocrystals in the experimental setting. Also, we obtained the following HOMO–LUMO gaps: Zn_3–Cr–O_4, 1.77; Zn_2–Cr_2–O_4,1.47; and Zn–Cr_3–O_4,1.28, i.e., decreasing with increasing number of Cr atoms. HOMO–LUMO gaps of this kind of doped clusters are lower than that of Zn_4O_4 clusters. In other words, the doping of Cr atoms makes ZnO nanocrystals have better electric properties. The same rule, which has been proved with experimental spectra, applies to Cu- and Al-doped clusters—again consistent with the experimental results. Orbital transitions in Cr-ZnO and Cu-ZnO structures are d–d, but not d–p (Fig. 5). Moreover, it is d orbital of Cr to d orbital of Cr atoms too. For Al-ZnO clusters, the transitions are s–p. Obviously, doping changes the properties of the luminescent characteristics of ZnO nanocrystals.

Conclusions

This paper reports an investigation into four ZnO cluster structures: Zn_3O_3, $(Zn_3O_3)_2$, $(Zn_3O_3)_3$ and Zn_4O_4. Absorption and Raman spectra of these clusters were found to be similar to those of experimental ZnO nanocrystals. The IR spectra of Zn_4O_4 structures were also similar to previously reported experimental data. Calculations with O–Zn–SR shows that the seven clusters have similarly optimized properties, which are identical with experimental findings: nanocrystals synthesized with ligands of thiol have the same properties. We also found that both solvent and ligands provoke a shift in the wavelengths of absorption peaks to blue. Moreover, all transitions of absorption peaks are from HOMO to LUMO, viz. from d to p orbitals. Finally, we studied Cr-, Cu- and Al-metal doping in ZnO. We demonstrated the existence of metal–metal bonds in Zn_2–Cr_2–O_4 molecules. Moreover, the transitions in Cr–ZnO

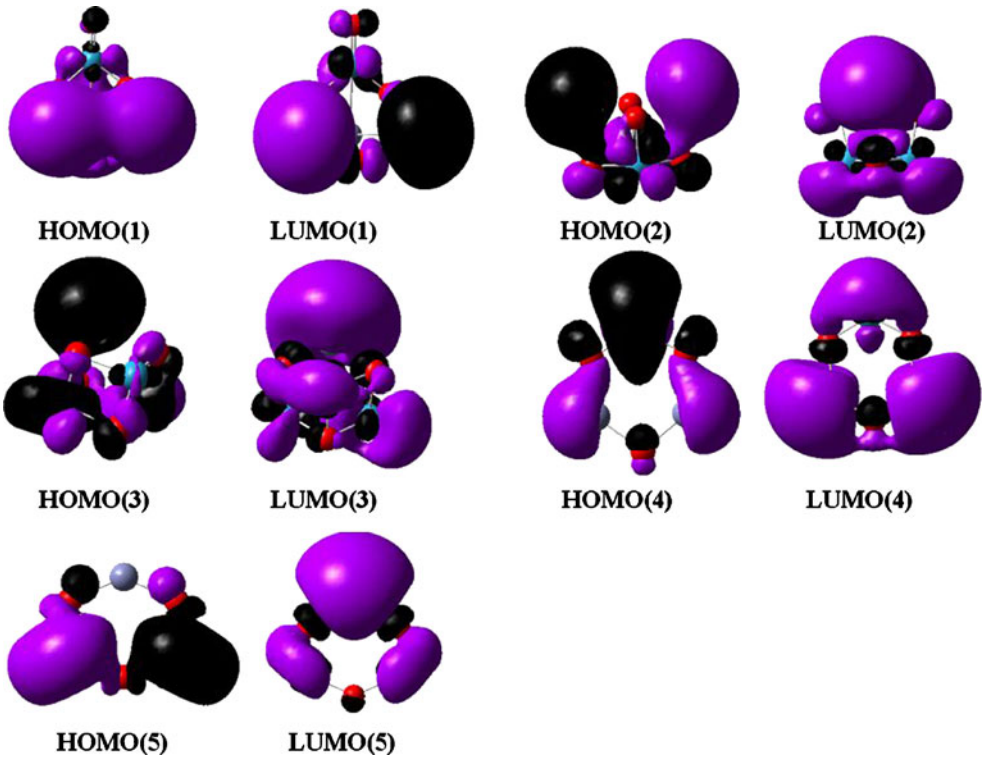

Fig. 5 HOMO and LUMO figures of Zn_3–Cr–O_4, Zn_2–Cr_2–O_4, Zn–Cr_3–O_4, Zn_2–Cr–O_3, Zn–Cr_2–O_3 molecules

and Cu–ZnO were identified as being d–d, while s–p transitions occur in Al–ZnO clusters.

Acknowledgment This work was supported by the National Natural Science Foundation of China under Grant No.60877024.

References

1. Yuan D, Wang GS, Xiang Y, Chen Y, Gao XQ, Lin G (2009) J Alloy Compd 478:489–492
2. Dmytruk A, Dmitruk I, Blonskyy I, Belosludov R, Kawazoe Y, Kasuya A (2009) Microelectron J 40:218–220
3. Antony J, Chen XB, Morrison J, Bergman L, Qiang Y, McCready DE, Engelhard MH (2005) Appl Phys Lett 87:241917
4. Wu S, Xu H, Xu H, Wang X, Schelly ZA (2006) Nanotechnology 17:4713–4718
5. Zhang R, Yin PG, Wang N, Guo L (2009) Solid State Sci 11:865–869
6. Cheng AJ, Tzeng Y, Xu H, Alur S, Wang Y, Park M, Wu T, Shannon C, Kim DJ, Wang D (2009) J Appl Phys 105:073104
7. Gao D, Zhang Z, Fu J, Xu Y, Qi J, Xue D (2009) J Appl Phys 105:113928
8. Ho C, Li J, Chen Y, Wu C, Huang Y, Tiong K (2009) J Alloys Compd 480:50–53
9. Guell F, Osso JO, Goni AR, Cornet A, Morante JR (2009) Superlattices Microstruct 45:271–276
10. Chassaing PM, Demangeot F, Combe N, Macary LS, Kahn ML, Chaudret B (2009) Phys Rev B 79:155314
11. Xiao Q, Ouyang L (2009) J Alloys Compd 479:L4–L7
12. Yadav MK, Sanyal B, Mookerjee A (2009) J Magn Magn Mater 321:273–276
13. Wang Z, Geng D, Hu W, Zhang Z (2009) J Appl Phys 105:123902
14. Wei L, Li Z, Zhang WF (2009) Appl Surf Sci 255:4992–4995
15. Li J, Hao W, Xu H, Wang T (2009) J Appl Phys 105:053907
16. Kumar S, Kumar R, Singh DP (2009) Appl Surf Sci 255:8014–8018
17. Xu X, Cao C (2009) J Magn Magn Mater 321:2216–2219
18. Ran FY, Imaoka M, Tanemura M, Hayashi Y, Herny TS, Lau SP (2009) Phys Status Solidi B 246:1243–1247
19. Lo SS, Huang D, Tu CH, Hou CH, Chen CC (2009) J Phys D Appl Phys 42:095420
20. Jang MS, Ryu MK, Yoon MH, Lee SH, Kim HK, Onodera A, Kojima S (2009) Curr Appl Phys 9:651–657
21. Fink K (2006) Chem Phys 326:297–307
22. Iusan D, Sanyal B, Eriksson O (2006) Phys Rev B 74:235208
23. Zhao M, Xia Y, Tan Z, Liu X, Mei L (2007) Phys Lett A 372:39–43
24. Cheng X, Li F, Zhao Y (2009) J Mol Struct THEOCHEM 894:121–127
25. Sanville E, Bel B (2007) J Phys Rev B 76:085412
26. Palacios P, Sanchez K, Wahnon P (2009) Thin Solid Films 517:2448–2451
27. Frisch MJ, Trucks GW, Schlegel HB, Scuseria GE, Robb MA, Cheeseman JR, Montgomery JA Jr, Vreven T, Kudin KN, Burant JC, Millam JM, Iyengar SS, Tomasi J, Barone V, Mennucci B, Cossi M, Scalmani G, Rega N, Petersson GA, Nakatsuji H, Hada M, Ehara M, Toyota K, Fukuda R, Hasegawa J, Ishida M, Nakajima T, Honda Y, Kitao O, Nakai H, Klene M, Li X, Knox JE, Hratchian HP, Cross JB, Adamo C, Jaramillo J, Gomperts R, Stratmann RE, Yazyev O, Austin AJ, Cammi R, Pomelli C, Ochtersky JW, Ayala PY, Morokuma K, Voth GA, Salvador P, Dannenberg JJ, Zakrzewski VG, Dapprich S, Daniela AD, Strain MC, Farkas O, Malick DK, Rabuck AD, Raghavachari K, Foresman JB, Ortiz JV, Cui Q, Baboul AG, Clifford S, Cioslowski J, Stefanov BB, Liu G, Liashenko A, Piskorz P, Komaromi I, Martin RL, Fox DJ, Keith T, Al-Laham MA, Peng CY, Nanayakkara A, Challacombe M, Gill PMW, Jonson B, Chen W, Wong MW, Gonzalez C, Pople JA (2004) Gaussian 03, Revision B03. Gaussian Inc, Wallingford CT
28. Amin EA, Truhlar DG (2008) J Chem Theory Comput 4:75–85
29. Yang Y, Weaver MN, Kenneth MM Jr (2009) J Phys Chem A 113:9843–9851
30. Weaver MN, Yang Y, Kenneth MMJ (2009) J PhysChem A 113:100081–10088
31. Goswami N, Sharma DK (2010) PhysE 42:1675–1682